Two-dimensional halide perovskite single crystals: principles and promises

Two-dimensional halide Perovskite Single Crystals: Principles and Promises

Cite this article as: Nishi Parikh, Mohammad Mahdi Tavakoli, Manoj Pandey, Manoj Kumar, Daniel Prochowicz, Rohit D. Chavan, Pankaj Yadav, Two-dimensional halide Perovskite Single Crystals: Principles and Promises, *Emergent Materials*, doi: 10.1007/s42247-021-00177-7

Two-dimensional halide Perovskite Single Crystals: Principles and Promises

Nishi Parikh,[a] Mohammad Mahdi Tavakoli,[b] Manoj Pandey,[a] Manoj Kumar,[c] Daniel Prochowicz,[d] Rohit D. Chavan,[e] Pankaj Yadav [f]**

[a] *Department of Chemistry, School of Technology, Pandit Deendayal Petroleum University, Gandhinagar-382 007, Gujarat, India*

[b] *Department of Electrical Engineering and Computer Science, Massachusetts Institute of Technology, Cambridge, MA 02139, USA*

[c] *Department of Physics, School of Technology, Pandit Deendayal Petroleum University, Gandhinagar-382 007, Gujarat, India*

[d] *Institute of Physical Chemistry, Polish Academy of Sciences, Kasprzaka 44/52, 01-224 Warsaw, Poland*

[e] *Polymer Energy Materials Laboratory, School of Applied Chemical Engineering, Chonnam National University, Gwangju 61186, South Korea*

[f] *Department of Solar Energy, School of Technology, Pandit Deendayal Petroleum University, Gandhinagar-382 007, Gujarat, India*

E-mail: Manoj.kspv@gmail.com; pankaj.yadav@sse.pdpu.ac.in

Abstract:

In last few years, two-dimensional halide perovskites are gaining tremendous attention and are replacing their 3D congeners rapidly. Owing to their greater stability and advantages of unique layered structure, intensive research has been done on 2D polycrystalline films. However, single crystals based on two dimensional halide perovskites are still emerging and has great potential for future device applications. Along with the hybrid halide perovskites, the all inorganic halide perovskites are also blossoming. In this review, we have discussed exclusively the development of hybrid as well as all inorganic two dimensional halide perovskites. First, we have discussed the crystal structure of 2D perovskites. In the next section, different growth procedures reported for preparation of single crystals are discussed. We then highlight the effect of doping on single crystals and their optoelectronic properties. Finally, we discuss the current challenges and future perspectives to further develop 2D single crystals for their efficient use in various devices.

Two-dimensional halide Perovskite Single Crystals: Principles and Promises

Abstract:

In last few years, two-dimensional (2D) metal halide perovskites (MHPs) are gaining tremendous attention and are replacing their three dimensional (3D) congeners rapidly. These next generation halide perovskites can circumvent the limitations of the 3D MHPs such as stability and structural diversity. The incorporation of bulky organic cation can not only prevent the moisture penetration into the crystal lattice and thus providing greater stability but it also expands the field of hybrid semiconducting materials by offering structural diversity. These unique features render even higher tuneability and improved photophysical properties and as a result intensive investigations have been made for 2D MHPs based polycrystalline thin films. However, single crystals based on two dimensional halide perovskites are still emerging and has great potential for future device applications. Along with the hybrid halide perovskites, the all inorganic halide perovskites are also blossoming. In this review, we have discussed exclusively the development of hybrid as well as all inorganic two dimensional halide perovskites. First, we have discussed the crystal structure of 2D perovskites. In the next section, different growth procedures reported for preparation of single crystals are discussed. We then highlight the effect of doping on single crystals and their optoelectronic properties. Finally, we discuss the current challenges and future perspectives to further develop 2D single crystals for their efficient use in various devices.

Keywords: Two dimensional Peorvskites, Single crystals, Crystal growth, Doping

1. Introduction

Astonishing development of solar cells technology has been led by 3D metal halide perovskites (MHPs) during the last 10 years.[1] Over the course of time the certified power conversion efficiency (PCE) of perovskite solar cells (PSCs) has reached to 25.5%,[2] which is comparable to the technologies based on CIGS, GaAs and silicon. As a result, significant efforts have been made for the commercialization of MHPs based devices using interface engineering,[3] compositional and crystal engineering,[4] surface passivation[5] and band alignment engineering.[6] This success stems from their obvious properties such as high absorption coefficient[7], tuneable band gap[8], sufficiently long carrier diffusion lengths[9]

easy solution processibility[10] etc. The unprecedented properties are a steep absorption onset[7] and significantly low non-radiative recombination rates. To date, many intensive investigations have been based on polycrystalline thin films.[11,12] With in-depth research, single crystals (SCs) of MHPs have been found to exhibit superior optoelectronic properties compared to polycrystalline counterparts.[13,14] There has been a lot of progress in the case of 3D MHP SCs i.e. from growth methods to unambiguous investigation of properties and application in different devices.[15–18] For example, Dong et. al., prepared millimeter-sized $MAPbI_3$ SCs via a low-temperature solution approach, in which a carrier diffusion length of over 175 μm was realised which is two orders of magnitude higher than the polycrystalline thin films.[19,20] In turn, Shi et. al., demonstrated the low trap-state density of states with an order of 10^9–10^{10} cm^{-3} and carrier diffusion length > 10 mm in $MAPbX_3$ single crystals.[21] It is found that SCs possess longer carrier diffusion lengths and greater stability owing to the absence of grain boundaries and reduced trap density. Nevertheless, the key issue in the real world application is the low stability of 3D MHPs towards elevated temperature and humidity.[22–24]

One of the effective ways to increase the environmental stability of 3D MHPs is to reduce the dimensionality. More stable two dimensional (2D) MHPs have effectively replaced the 3D ones in recent years.[25–28] The greater stability of 2D MHPs accounts for the bulky hydrophobic organic spacer cation, which prevents moisture penetration in the crystal structure.[29] Apart from this advantage, spacer cation also provides structural diversity to the 2D MHPs which provides opportunities for chemical engineering of these materials to make them suitable for wider range of applications. The other properties of 2D MHPs are their tuneable bandgap (E_g) which generally decreases with increasing layer thickness (n).[30] Owing to this compositional tuning of bandgap, the targeted application of 2D MHPs is possible.[31] Significant efforts are being made for the thorough understanding of their structure-property relationships, carrier dynamics and orientation control.[32–34] Both the organic-inorganic hybrid (OIHP) as well as all inorganic 2D MHPs are gaining tremendous momentum and are becoming fast growing field.[35,36] However, the SCs of 2D MHPs are still lagging behind the 3D SCs and are in their initial stage of development.

In this review, we have summarised exclusively the development in the field of both OIHP and all inorganic 2D MHP SCs. First, we have discussed the crystal structure of 2D MHPs, followed by the detailed discussion on the growth methods of SCs with their merits and demerits. (Scheme 1) Thereafter we have discussed the effect of doping on the 2D SCs. In

next section, we have highlighted their promising physical properties particularly the bandgap and carrier transport properties. At last, future scopes for the development in this field are proposed.

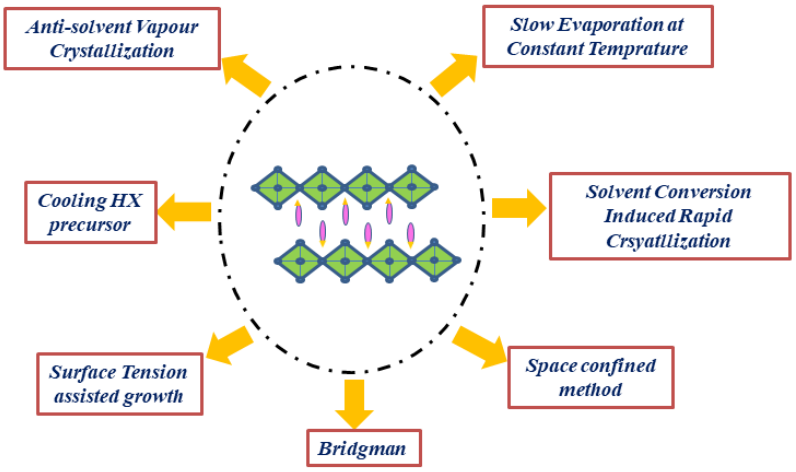

Scheme 1: Schematic of different growth methods of 2D MHPs. Reprinted from ref. no. [37]

2. Crystal Structures of 2D MHPs

The conventional 3D MHPs are represented by the general formula ABX_3 where B is a divalent metal cation (e.g. Pb^{2+}, Sn^{2+}) and X is the halogen anion (e.g. I^-, Br^-, Cl^-). The twelve A-site cations (e.g. MA^+, Cs^+, FA^+) are situated at the centre of the four BX_6 octahedra.[38] The stability of this compounds are defined by the Goldschmidt tolerance factor (*t*), the value of which should be ideally ~ 0.8 to 1.[39] Owing to this geometric consideration, several restrictions are imposed on the 3D MHPs such as structural diversity. This criterion is overlooked in the case of 2D layered perovskites. It is worth to note that 2D structure can be formed by either morphological tuning to produce thin layered perovskites[40–42] (e.g. using long-chain organic ligand templated growth, self-templated growth) or by the crystallographical slicing of 3D MHPs. The general formula for 2D MHPsis $(A')_m(A)_{n-1}B_nX_{3n+1}$, where A' is an arbitrarily long organic spacer cation which cleaves the 3D structure to form layered structure.[43][44] (Figure 1a) Similar to the 3D MHPs, the growth of 2D MHPs is also governed by stereochemical rules. There have been three octahedral connectivity modes observed: edge-sharing, corner-sharing and face-sharing. The connectivity modes affect the orbital overlap which in turn governs the band gap of the material. It has been established theoretically and experimentally that the general trend of band gap observed is: "corner-sharing < edge-sharing < face-sharing. However, the main class of 2D MHPs consists of the compound with corner-sharing octahedra, which is further

classified into the <100>-oriented, <110>-oriented and <111>-oriented 2D perovskites (Figure 1b).

The 3D structure of perovskite can be sliced down along the <100>, <110> and <111> crystallographic planes, which divide the 2D perovskites into three classes:

The <100>-oriented class of 2D MHPs are represented by general formula $(RNH_3)_2A_{n-1}B_nX_{3n+1}$. Structurally, they can be described as flat inorganic sheets with different layer thickness (*n*) along the <100> direction with respect to parent structure. This class offers higher degree of compositional diversity and is the most studied class of 2D perovskites.[26] It can be sub classified into Ruddelsden-Popper (RP) and Dion-Jacobson (DJ) type perovskites *(vide infra).* Apart from this, all-inorganic compounds ($Cs_2PbI_2Cl_2$, $Cs_2SnI_2Cl_2$) and hybrid compounds ($(MA)_2PbI_2(SCN)_2$) represent peculiar derivatives of K_2NiF_4 (structural similarities with Ruddelsden-Popper class) prototype. In these compounds, the lattice positions along the perovskite plane and vertically to it are occupied by different chemical species and generally the larger atoms (i.e. I^- in all-inorganic and SCN^- in hybrid) are present on the surface of the layers whereas the smaller atoms take part in the expansion of the corner sharing octahedra. These compounds are drastically different than the other hybrid organic-inorganic compounds because in this the layered structure is not obtained due to the bulky organic spacer but rather it forms naturally possibly because of the ionic size mismatch.

When the 3D MHPs are cut along the <110> direction, the <110>-oriented family is obtained having general formula $A_2A'_mB_mX_{3m+2}$, m > 1. This class offers interesting behaviours to study one of which is white light emission at room temperature. This can be due to the distorted inorganic sheets obtained from the face diagonal of the parent 3D structure. However, only handful of examples are reported on the utilisation of this family as light absorber layer plausibly because of the difficulty in tuning inorganic sheets and limited spacer cations that can stabilise the structure.[30] The <111>-oriented 2D perovskites are obtained when the 3D perovskite is sliced from the body diagonal and possess general formula $A'_2A_{q-1}B_qX_{3q+3}$ (q > 1). The typical examples of this class is $Cs_3B_2X_9$ (q=2, $A_3B_2X_9$) where B^{3+} is group 15 ions e.g. Bi, Sb, As. These materials are rarely studied owing to their strong excitonic nature which deteriorates the performance of solar cells.[45]

2.1. Ruddelsden-Popper and Dion-Jacobson type 2D perovskites:

RP type perovskite can be visualised to be formed from the 3D ABX_3 and 2D $(R\text{-}NH_3)_2BX_4$, resulting into $(R\text{-}NH_3)_2A_{n-1}B_nX_{3n+1}$. Crystallographically, it shows (½, ½) displacement along *ab*-plane and hence possess staggered configuration.[26] The $R\text{-}NH_3$ is an organic cation which can be alkyl or aryl ammonium such as butylammonium[46], phenylethyl ammonium[35], to mention a few. Van-der-Waals force exists between the bilayer of the monovalent cation and adjacent inorganic sheets. Similar to the RP perovskites, DJ perovskite owe their name to their oxide perovskite analogues due to the structural similarities. In this type, bivalent cation is present between the inorganic sheets and so there is no displacement along *ab*-plane or has (½, 0) shift. [26] The inorganic layers are stacked exactly on top of each other. The typical examples of spacer cations which forms DJ perovskite are 3-AMP [3-(aminomethyl)piperidinium], 4-AMP [4-(aminomethyl)piperidinium][47] etc. (Figure 1c).

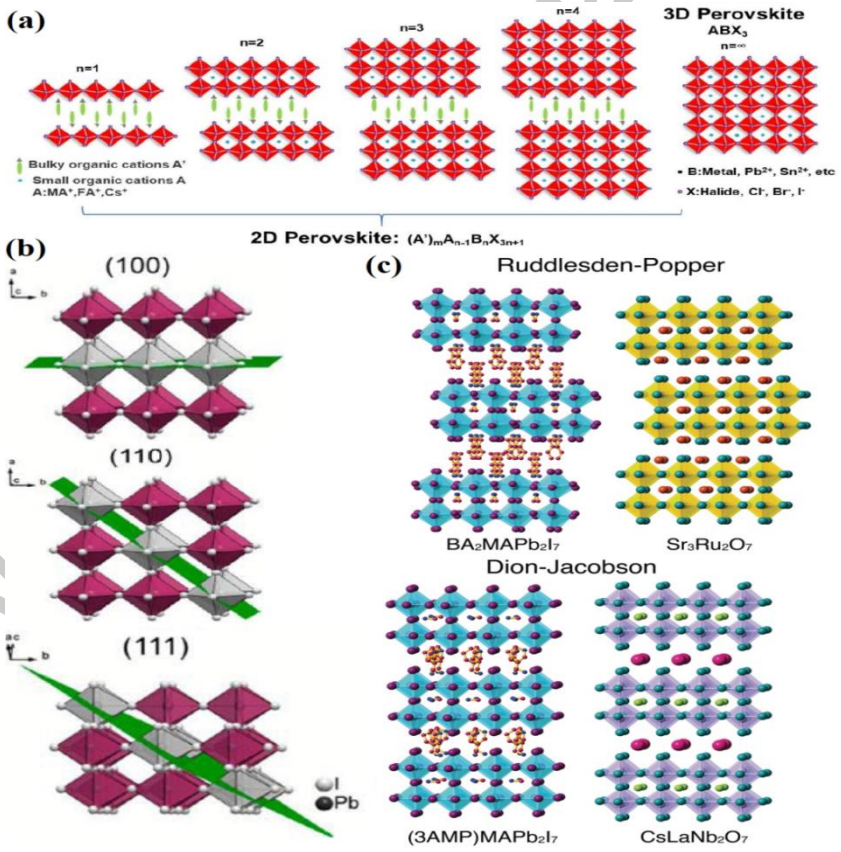

Figure 1: (a) Schematic of comparison of 2D and 3D perovskite structures Reprinted with permission from ref no [25], Copyright 2020 The Royal Society of Chemistry (b) Schematic illustration of the cuts along 100, 110 and 111 planes and deriving the 2D perovskites from

such cuts Reprinted with permission from ref. no. [26], Copyright 2019 The Royal Society of Chemistry (c) Comparison of RP and DJ type oxide and halide perovskites. Reprinted with permission from ref. no. [48], Copyright 2019 Wiley-VCH .

3. Methods for the MHP SCs formation

In this section, various methods to prepare both OIHP and all-inorganic 2D MHP SCs are discussed.

3.1 Growth methods of 2D OIHP SCs

As compared to the crystallization process of 3D MHPs, the process for the synthesis of 2D MHPs is complex and tricky. The important factors, which contribute in the crystallization of 2D MHP SCs are careful control of temperature, choice of solvent and adequate amount of precursors to control layer and phase purity.

3.1.1. Cooling the Hydrohalic acid (HX) based precursor

This method was first used by Poglitsch et. al., in 1987 to prepare single crystals of 3D $CH_3NH_3PbX_3$ (X = I, Br, Cl).[49] Later, Dang et. al., have also followed this method for the preparation of millimetre sized $CH_3NH_3PbI_3$ crystals by cooling the aqueous solution to 40^oC.[50] In the case of $CH_3NH_3PbI_3$, below 40^oC formation of $CH_3NH_3PbI_3{\cdot}H_2O$ begins. The method also works for the preparation of 2D OIHP SCs. The SCs of the homologous series of $(BA)_2(MA)_{n-1}Pb_nI_{3n+1}$ (n = 1,2,3,4,∞) were prepared by cooling the precursors solution in aqueous HI to room temperature.[51] However, the as-synthesized crystals were very small as the cooling rate was not controlled in this report. Therefore, the important factor is the careful control of cooling for the synthesis of large sized and high quality 2D SCs. In case of rapid cooling many nucleation sites appear, leading to large number of small crystals (Figure 2). Peng et. al., prepared milimeter scale SCs of $PEA_2PbI_4{\cdot}(MAPbI_3)_{n-1}$ (n = 1, 2, 3) by cooling the aq. HI solution at a rate of 1^oC/h from 90^oC.[52] However, the crystals with $n > 3$ are produced as a mixture of lower n-members owing to the large difference in the solubility of PEAI and MAI in HI. The authors proposed that due to the inclusion of large sized organic spacer cation during crystallisation, the overall defect density decreases and high quality crystals are produced. The self-assembly nature of organic cation, large size and high molecular mass suppresses defects arising from small sized MA^+. Additionally, this method was also used to prepare SCs of 2D DJ type OIHPs by Mao et. al.[53] They prepared

SCs of homologous series of (A') $(MA)_{n-1}Pb_nI_{3n+1}$ where A' is 3-AMP [3-(aminomethyl)piperidinium] and 4-AMP [4-(aminomethyl)piperidinium] and *n* = 1 to 4.

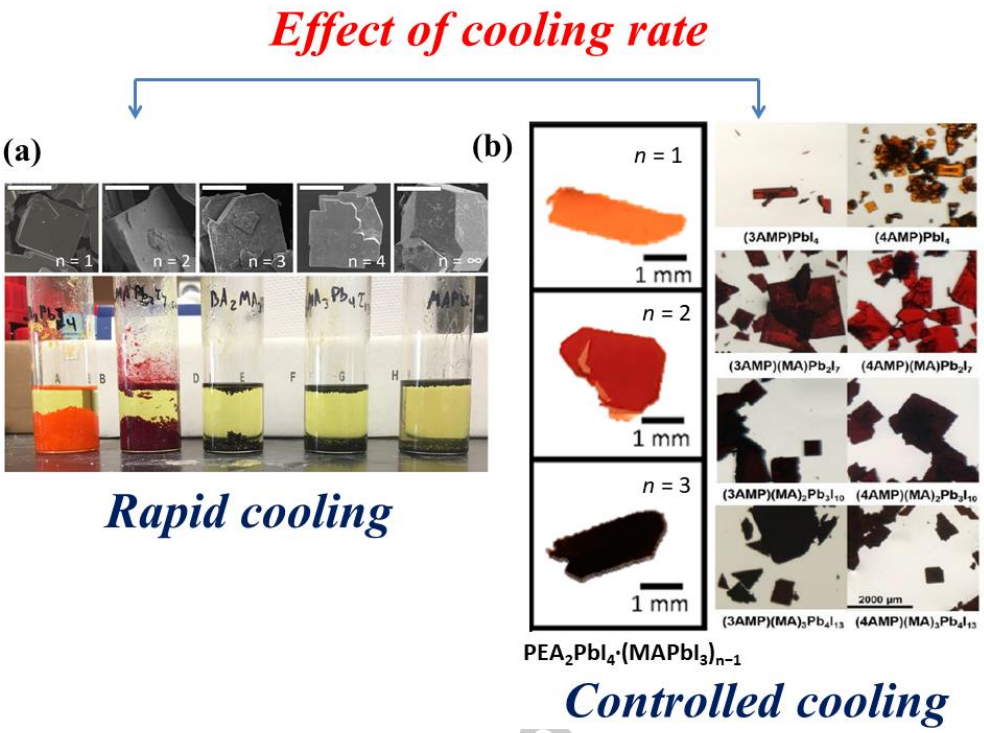

Figure 2: The effect of cooling rate on the crystallization (a) SEM images (top) and photographs of the $(BA)_2(MA)_{n-1}Pb_nI_{3n+1}$ perovskite crystals (bottom) (scale bars = 200 μm). Reprinted with permission from ref no [51], Copyright 2016 American Chemical Society (b) Optical images of crystals of $PEA_2PbI_4{\cdot}(MAPbI_3)_{n-1}$ (*n* = 1, 2, 3) (left) and (3-AMP) $(MA)_{n-1}Pb_nI_{3n+1}$; (4-AMP) $(MA)_{n-1}Pb_nI_{3n+1}$ (right). Reprinted with permission from ref no [52], Copyright 2017 American Chemical Society and Reprinted with permission from ref no [53], Copyright 2018 American Chemical Society

3.1.2. Slow evaporation at constant temperature (SECT)

This method was first introduced by Raghavan et. al., for the synthesis of well-shaped SCs of 2D OIHP with the high phase purity.[54] Unlike the controlled cooling method in which randomly stacked flakes are formed, here the nucleation is controlled. As a result, stacking in crystals is prevented. The step wise procedure is shown in Figure 3a. First, the saturated precursor solution is prepared in HI and then the solvent is evaporated at a particular temperature. At the bottom of this now super-saturated solution, the excess solutes start crystallizing and this event drove the crystal growth process. After careful control of evaporation rate well facet plate like crystals of $(BA)_2(MA)_{n-1}Pb_nI_{3n+1}$ (*n* = 1, 2, 3) are

formed. In another report by Zhang et. al., $(PEA)_2PbBr_4$ SCs were prepared using this method and were suitable for the fabrication of UV-detector.[55] Figure 3b and c provides clear insight into the crystallization process involved in this method. As shown in the mass-loss curve (figure 3b), initially only the solvent gets evaporated and no crystallites are formed. The intersection point of the two lines shows the critical concentration of $(PEA)_2PbBr_4$. After this point the crystallization occurred. The disadvantage of this method is that it takes too long time for the crystal growth.

3.1.3. Anti-solvent vapour assisted crystallization

The method of fast crystallization[56] and solvent engineering[57] were previously introduced and used for the preparation of high quality OIHP thin films. The strategy of this method is based on the solubility difference of perovskite precursors in different solvents. The good solvent used for perovskites are N,N-dimethylformamide (DMF), dimethylsulfoxide (DMSO) and γ–butyrolactone (GBL), while the poor solvents (anti-solvent) are dichloromethane (DCM), chlorobenzene etc. Using this concept, Bakr's group reported a novel method to prepare SCs of 3D OIHPs.[21] In case of SCs, the vapour of antisolvent diffuses in the solution and mixes well with the solvent. However, the solutes (MABr, $PbBr_2$) do not solubilize with the anti-solvent. As a result the concentration of solutes increases in the solvent and crystallization proceeds. Tian et. al., used this method for the synthesis of 2D PEA_2PbBr_4 SCs using DMF as solvent and cholorobenzene as antisolvent (Figure 2d).[58] The crystals with a size of few millimetres were obtained after several days (Figure 3e and f). To get single crystalline thin films, Lédée et. al., developed "Anti-solvent Vapor-assisted Capping Crystallization" (AVCC) method by combining AVC method and space confined method (Figure 3g).[59] This approach yields in high quality SCs of PEA_2PbI_4 with thickness in micrometre scale in 30 minutes using DCM as antisolvent (Figure 3h). These results demonstrated that GBL allows better crystallization than DMF as a solvent (Figure 3i and j).

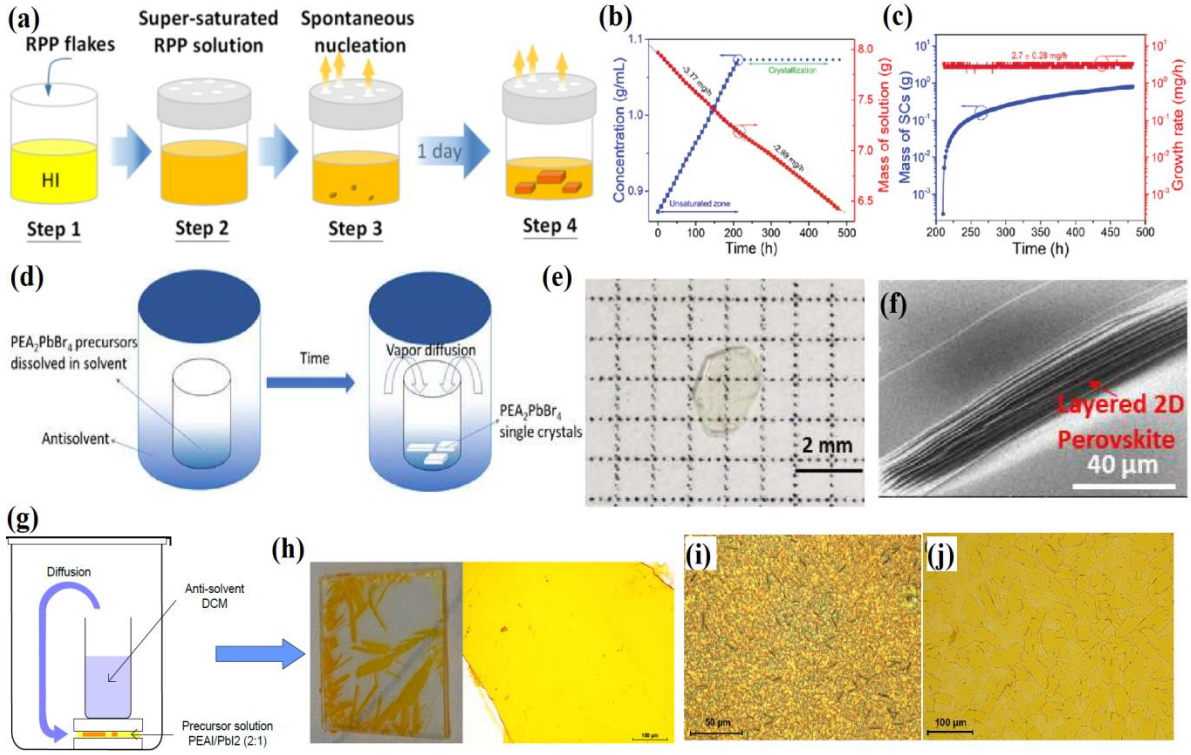

Figure 3: (a) Schematic illustration of the steps involved in SECT method Reprinted with permission from ref no [54], Copyright 2018 American Chemical Society (b) Mass and concentration of $(PEA)_2PbBr_4$ precursor solution as a function of evaporation time (c) Mass and growth rate of $(PEA)_2PbBr_4$ as a function of time Reprinted with permission from ref no [55], Copyright 2019 The Royal Society of Chemistry (d) Schematic illustration of AVC method (e) Optical image of $(PEA)_2PbBr_4$ SC (f) SEM image of the $(PEA)_2PbBr_4$ SC showing layered structure Reprinted with permission from ref no [58], Copyright 2017 American Chemical Society (g) Schematic of AVCC method (h) Photograph of the $(PEA)_2PbI_4$ SC prepared using AVCC method Optical images of the monocrystalline thin film of $(PEA)_2PbI_4$ prepared (i) using DMF as solvent (j) using GBL as solvent Reprinted with permission from ref no [59], Copyright 2017 The Royal Society of Chemistry

3.1.4. Surface Tension Assisted Growth

It is known that the nucleation barrier at the solution surface is lower than the solution and therefore, the nucleus formation is more likely to form at the surface than in the solution (Figure 4a and b).[60] Taking advantage of this fact, Liu et. al., synthesized SCs of $(PEA)_2PbI_4$ with size of 36 mm using GBL as solvent.[61] At higher temperature (105^{o}C) the precursors solubilize in solvent but as the temperature is decreased (0.5^{o}C/h), small crystallite started forming at 95^{o}C. As the temperature decreasing more rectangular block shaped crystal

are formed at 30°C (Figure 4c and d). Wang et. al., prepared SCs of $(BA)_2(CH_3NH_3)_{n-1}Pb_nI_{3n+1}$ (n=1, 2, 3, 4 and ∞) from the water-air interface.[62] The report suggests that water as a solvent improves the growth rate and floatation of the crystal owing to its higher surface tension coefficient of 72.86 $mN \cdot m^{-1}$ than commonly used organic solvents such as DMSO (σ = 42.8 $mN \cdot m^{-1}$) or DMF (σ = 35.2 $mN \cdot m^{-1}$). Moreover, the self-assembly nature of spacer cation acts as the template for the growth of crystal during crystallization at water-air interface.

3.1.5. Space confined method

The advantage of this method over the other methods is that it allows the growth of crystal with controllable thickness. In this method, the crystal is allowed to grow in between the two substrates (e.g. glass slides). The method is effectively used to prepare single crystalline thin films of 3D OIHPs.[63][64] Xiao et. al., used this method to prepare SCs of $BA_2MA_2Pb_3I_{10}$ by confining the precursor solution between two non-wetting substrates.[65] Liu et. al., used this method to synthesize multi inch sized single crystalline perovskite membrane of PEA_2PbI_4 for sensing.[66] The brief process includes preparing the solution of 2.12 M at 80°C in GBL and pipetted on the PET substrate. Then another glass slide is placed on top of it such that part of the solution squeeze out to the edge of top slide (Figure 4e). This edge of the second slide provides nucleation site to direct the growth of the crystals inward rather than forming nanocrystals. Then gradient cooling at the rate of 1°C/h up to 53°C produces multi inch single crystal. He et. al., synthesized SCs of $(BA)_2(MA)_{n-1}Pb_nI_{3n+1}$ (n = 1,2,3) using modified space confined method with the lateral size reaching millimeter, the thickness about 400-1000 nm and the quantum well layers being parallel to the substrate.[67] At 80°C, after the H_2O and HI solution evaporates single crystal membrane can be obtained between the two glass slides. Apart from this, Gu et. al., presented a general seed printing approach for the synthesis of single crystalline film with controllable thickness.[68] The method can prevent random crystallization by affecting the mass transport and distribution of perovskite precursor ions.

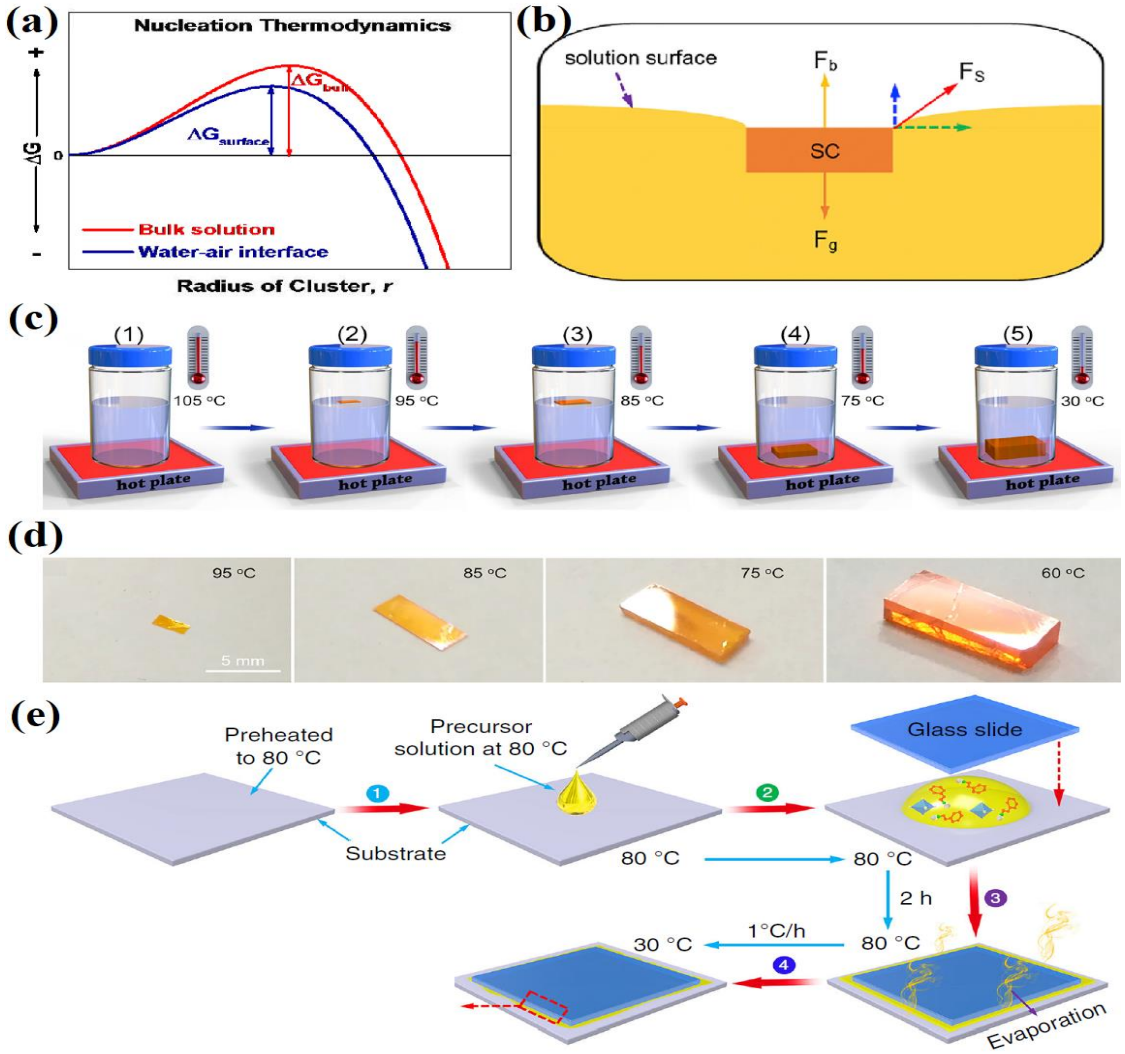

Figure 4: (a) Graphical illustration of the lower nucleation barrier at surface Reprinted with permission from [62], Copyright 2018 American Chemical Society (b) Schematic of the single crystal staying afloat on the solution surface (c) Schematic of the surface tension assisted growth of crystal (d) Corresponding photographs of $(PEA)_2PbI_4$ PSCs completed at different temperatures Reprinted with permission from ref no [61], Copyright 2019 Elsevier Publishing group and (e) schematic illustration of space confined method Reprinted with permission from ref no [66], Nature publishing group

3.1.6. Other methods

Wang et. al., presented a novel economic and universal aqueous synthesis for the preparation of SCs of lower dimensional halide perovskites.[69] The method uses deionized water as solvent instead of DMF or DMSO, which are highly toxic. Additionally, the intentional heating of the solution is avoided as the method yields SCs at room temperature. The schematic of the steps involved are shown in Figure 5a. First, PbI_2 powder is mixed with

water, however, the solubility of PbI_2 is extremely low in water. After addition of HI it gets dissolved. In this method, pH is of vital importance. At pH < 4, the mixture of MAI and R-NH_3I is added while stirring. Then, the solution is left overnight to grow crystals (Figure 5b). In another report, Fateev et. al., reported a universal strategy to synthesize of both 3D and 2D SCs perovskites i.e. Solvent Conversion-Induced Rapid Crystallization (SCIRC) (Figure 5c).[70] The method is based on the selection of a pair of solvents, which can slowly react with each other and irreversibly because of that reaction the perovskite precursor get dissolved. The reaction produces as solvent in which the resultant crystals are insoluble. The typical example of this reaction can be given as the hydrolysis reaction of cyclic carbonate and water in acidic media (e.g. HX acid) which produces glycols, an antisolvent for halide perovskites.

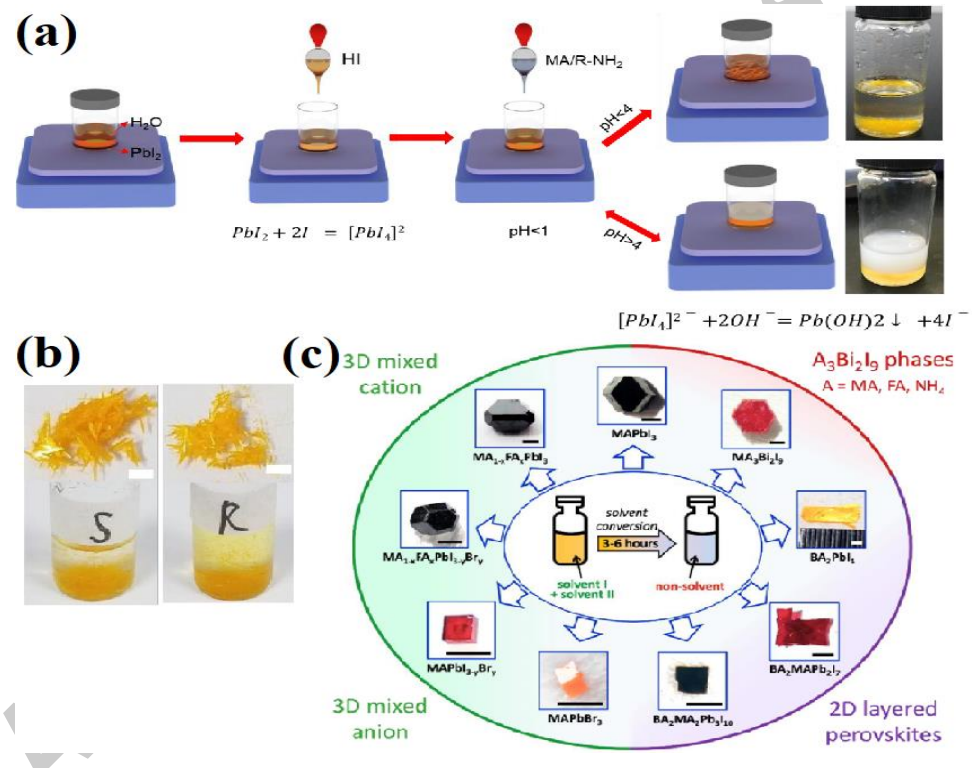

Figure 5: (a) Schematic illustration of the steps involved in the aqueous synthesis of SCs at room temperature (b) Photographs of the as synthesized SCs of S-α-PEA_2PbI_4 and R- α-PEA_2PbI_4 and Reprinted with permission from [69], Copyright 2019 American Chemical Society (c) Schematic and optical images of the SCs obtained via versatile SCIRC method Reprinted with permission from ref no [70], Copyright 2020 American Chemical Society

Table 1. A Summary of different growth methods and associated parameters for the synthesis of 2D OIHP SCs

Sr. No.	Formula of Perovskite	Name of Method	Ratio of precursors	Initial Temperature	Cooling Rate	Application	Ref
1.	PEA_2PbI_4	Cooling HX precursor	PbO : MA : PEA 1.72 : 0 : 3.75mmol	90°C	1°C/h	Photoconductor	[52]
2.	$PEA_2MAPb_2I_7$	Cooling HX precursor	PbO : MA : PEA 6 : 18 : 1mmol	90°C	1°C/h	Photoconductor	[52]
3.	$PEA_2MA_2Pb_3I_{10}$	Cooling HX precursor	PbO : MA : PEA 10 : 24 : 1mmol	90°C	1°C/h	Photoconductor	[52]
4.	BA_2PbI_4	Cooling HX precursor	PbO : MA : BA 10 : 0 : 10mmol	Boiling	Rapid cooling	-	[51]
5.	$BA_2MAPb_2I_7$	Cooling HX precursor	PbO : MA : BA 10 : 5 : 7mmol	Boiling	Rapid cooling	-	[51]
6.	$BA_2MA_2Pb_3I_{10}$	Cooling HX precursor	PbO : MA : BA 10 : 6.67 : 3.33mmol	Boiling	Rapid cooling	-	[51]
7.	$BA_2MA_3Pb_4I_{13}$	Cooling HX precursor	PbO : MA : BA 10 : 7.5 : 2.5mmol	Boiling	Rapid cooling	-	[51]
8.	(3-AMP)Pb_2I_4	Cooling HX precursor	PbO : MA : 3-AMP 3 : 0 : 3mmol	130°C		Solar Cell	[53]
9.	(3-AMP)$MAPb_2I_7$	Cooling HX precursor	PbO : MA : 3-AMP 3 : 2 : 0.5mmol	130°C		Solar Cell	[53]
10.	(3-AMP)$MA_2Pb_3I_{10}$	Cooling HX	PbO : MA : 3-AMP	130°C		Solar Cell	[53]

		precursor	3 : 3 : 0.33mmol			
11.	(3-AMP)$MA_3Pb_4I_{13}$	Cooling HX precursor	PbO : MA : 3-AMP 4 : 4 : 0.3mmol	130°C	Solar Cell	[53]
12.	(4-AMP)PbI_4	Cooling HX precursor	PbO : MA : 4-AMP 3 : 0 : 3mmol	130°C	Solar Cell	[53]
13.	(4-AMP)$MAPb_2I_7$	Cooling HX precursor	PbO : MA : 4-AMP 3 : 2 : 0.5mmol	130°C	Solar Cell	[53]
14.	(4-AMP)$MA_2Pb_3I_{10}$	Cooling HX precursor	PbO : MA : 4-AMP 3 : 3 : 0.33mmol	130°C	Solar Cell	[53]
15.	(4-AMP)$MA_3Pb_4I_{13}$	Cooling HX precursor	PbO : MA : 4-AMP 4 : 4 : 0.3mmol	130°C	Solar Cell	[53]
16.	BA_2PbI_4	SECT	PbO : MA : BA 10 : 0 : 10mmol (in HI/H_3PO_2)	62°C	-	[54]
17.	$BA_2MAPb_2I_7$	SECT	PbO : MA : BA 10 : 5 : 7mmol(in HI/H_3PO_2)	62°C	-	[54]
18.	$BA_2MA_2Pb_3I_{10}$	SECT	PbO : MA : BA 10 : 6.67 : 3.33mmol(in HI/H_3PO_2)	62°C	-	[54]

19.	PEA_2PbBr_4	SECT	$PbBr_2$: PEABr 2.01gm : 1.835gm (in DMF)	23°C	Photodetector	[55]
20.	PEA_2PbBr_4	AVC	$PbBr_2$: PEABr 1 : 2 M (in DMF)	Room temp	Memory Devices	[58]
21.	PEA_2PbI_4	AVCC	PbI_2 : PEAI 1 : 2 M (in GBL)	Room temp	Photodetector	[59]
22.	PEA_2PbI_4	Surface Tension assisted growth	PbI_2 : PEAI 1 : 2 M (in GBL)	105°C	0.5°C/h Photodetector	[61]
23.	$(BA)_2(CH_3NH_3)_{n-1}Pb_nI_{3n+1}$ (n=1, 2, 3, 4)	Surface Tension assisted growth	PbO : (MA + BA) 5 : 5mmol (in HI/H_3PO_2)	100°C	1°C/2h Photodetector	[62]
24.	$BA_2MA_2Pb_3I_{10}$	Space confined method	PbI_2 : MAI : BA 3 : 2 : 2 (in HI)	130°C	-	[65]
25.	PEA_2PbI_4	Space confined method	PbI_2 : PEAI 1 : 2 M (in GBL)	80°C	1°C/h Flexible Photosensor	[66]

3.2. Growth methods of 2D all-inorganic SCs

3.2.1. Bridgman method

McCall et. al., prepared and investigated SCs of $A_3M_2I_9$ (A = Cs, Rb; M = Bi, Sb) using Bridgman method.[71] Later the same group synthesized large SCs of $Cs_3Bi_2I_6Cl_3$ using this method.[72] The procedure involves mixing of CsCl and BiI_3 in ampule, which is placed in two-zone Bridgman furnace. The hot zone was kept at 725°C and cold zone at 300°C. After

12 h the ampule was dropped gradually to reach 300^{o}C. At last, cherry red ingot formed after several days, which had large SCs. Tarasova et. al., grew $K_xRb_{1-x}Pb_2Br_5$ SCs, with x = 0, 0.5 and 1.0 using the Bridgman technique in sealed quartz ampoules in halogen atmosphere(CBr_4).[73] The growth rate was 0.08 – 0.17 mm/h and duration of cooling to room temperature was 12 h. Using these parameters high-quality single-crystalline boules of KPb_2Br_5, $K_{0.5}Rb_{0.5}Pb_2Br_5$, and $RbPb_2Br_5$ with a diameter up to 15 mm and 40 mm length were obtained. Recently, Acharyya et. al., studied RP 2D $Cs_2PbI_2Cl_2$ SCs by cutting them in the direction parallel and perpendicular to the Bridgman growth direction (Figure 6a).[74] First, stoichiometric amount of PbI_2 and CsCl were melted in the sealed quartz tube. Then, the starting materials were heated at 923 K for 48 h. The melt was then pulled in a temperature gradient from 773 K to 623 K at a speed of 0.77 mm/h. Finally, the sample was slowly cooled to room temperature in 96 h.

3.2.2. Solution Methods

Li et. al., prepared the first all-inorganic layered perovskite white light-emitting material, $Rb_2CdCl_2I_2$ by a facile aqueous solution method.[75] Briefly, stoichiometric amounts of $CdCO_3$ and Rb_2CO_3 were added to the HCl/HI (1:1) solution and heated for 5 min and allowed to cool. After several days SCs of $Rb_2CdCl_2I_2$ are formed (Figure 6b). In other report, Dursun et. al., synthesized SCs of $CsPb_2Br_5$ using anti solvent vapour crystallization (AVC) method using DMSO and MeOH as solvent and anti-solvent pair.[76] The choice of anti-solvent is of vital importance as the final products of crystallization are defined by the miscibility of the solvent pair. The crystallization procedure is divided into two steps. In initial 48 h, $CsPbBr_3$ is formed because of the diffusion of MeOH in DMSO. After five weeks, the orange crystals grow and convert into transparent crystals of $CsPb_2Br_5$ (Figure 6c and d). Usman et. al., prepared $Cs_4FeBiBr_{10}$ a new type of MHP SC using a solution temperature lowering method.[77] First the metallic salts, $BiBr_3$, $FeCl_3$ and CsBr were dissolved in HBr at 120^{o}C and on cooling the solution to room temperature red coloured crystallites formed. To grow larger crystals the temperature cooling rate was controlled at 1^{o}C/hr and that resulted in crystals with dimension 4mm x 1mm x 1mm.

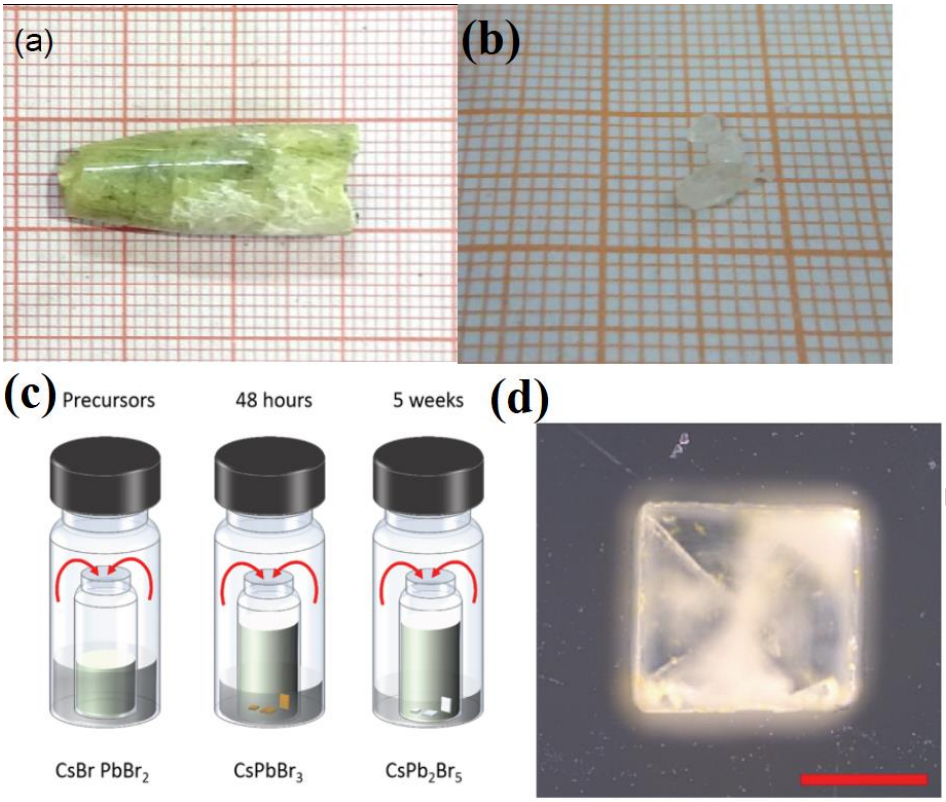

Figure 6: (a) Photograph of $Cs_2PbI_2Cl_2$ Bridgman grown crystal Reprinted with permission from ref no [74], Copyright 2020, American Chemical Society (b) Photograph of $Rb_2CdCl_2I_2$ SCs grown by aqueous solution method Reprinted with permission from ref no [75], Copyright 2018, Wiley-VCH (c) Schematic diagram of the $CsPb_2Br_5$ single crystal growing by AVC method (d) optical image of the $CsPb_2Br_5$ single crystal Scale bar 200 μm Reprinted with permission from ref no [76], Copyright 2017, Wiley-VCH

4. Doping in 2D MHP SCs

Doping is a general and effective strategy to modifying the fundamental properties of semiconductors in which the heteroatoms are intentionally introduced into the host lattice.[78,79] Unlike in the case of conventional inorganic semiconductors (e.g. Si, GaAs) where dopants create deep energy levels which act as electron traps, in case of MHPs, the dopants do not create mid-gap states.[80–82] The defect tolerant nature of MHPs not only equips the doped MHPs with expected optoelectronic properties but also provides an additional tool to modulate the structure and resulting performance. With this aim, various metal cations (e.g. Bi^{3+}, K^{+}, Mn^{2+}, Rb^{+} etc) have been doped into the MHPs and exotic properties are imparted such as enhanced stability, new emission characteristics, improved

PLQY etc.[83–88]However, handful of examples is reported on the effect of doping in the case of 2D MHP SCs.

In early days, the first report on Ni^{2+} doping was reported by Ghosh and Mukherjee in the all inorganic Cs_2CdCl_4 host crystals.[89] The crystals were shown to possess 2D layered structure and isostructural with K_2NiF_4. The important observation found in the study was the strong luminescence obtained at 16340 cm^{-1} and 12250 cm^{-1} at 77 K assigned to the $^1T_2(D) \rightarrow {}^3A_2(F)$ and $^1T_2(D) \rightarrow {}^3T_2(F)$ transitions of Ni^{2+}, respectively.

Biswas et. al., presented Mn^{2+} doping in the layered 2D $(BA)_2PbBr_4$ host material using solid state grinding technique.[90] The results demonstrated that there is an efficient energy transfer from photoexcited host ions to dopant ions due to higher confinement of excitons in 2D perovskites and higher covalency in Mn-Br bond enhancing sp-d exchange interaction in 2D perovskites. Similarly, the effect of Mn-doping is studied by dissolving the undoped crystal by forming nanocrystals or thin films.[91] However, in a report by Sheikh et. al., Mn-doped $(BA)_2PbBr_4$ SCs were synthesized by modifying the acid precipitation method and studied their optical properties.[92] Although centimetre sized crystals were prepared, very small fractions of Mn-precursor are found in final product because of the difficulty in Mn-doping.[93] They also exfoliated few layers of SCs using the well-known scotch tape method. As shown in Figure 7a, as the Mn concentration increases the intensity of Mn emission increases whereas the intensity of excitonic emission decreases systematically. The reason can be attributed to the reduced surface defects in SCs. The other important conclusion of the report is that exciton intensity is dependent on the Mn-emission intensity of a SC i.e. stronger Mn emission is observed when the energy of the excitation light is equal to the bandgap of host material and because it travel deeper into the crystal.

Zhang et. al., presented the effect of Bi doping in the lead free PEA_2SnBr_4 SCs.[94] The $PEA_2Sn_{1-x}Bi_xBr_{4+x}$ ($x << 1$) SCs were prepared using cooling induced precipitation method. It was observed in the photoluminescence (PL) spectra that blue shifting of the PL peaks occurs as the Bi doping concentration is increased. Moreover, the low energy tail also weakens and is completely absent in case of 10% and 20% doping concentration (Figure 7b). These features can be attributed to the photon recycling effect and quenching of radiative self-trapped states.[95][96]

Cervantes et. al., prepared 2D $[DDA]_2PbBr_4$ (1-as) where DDA is deca-3,5-diyn-1-amine.[97] Then, the polymerization was induced by heating in inert atmosphere (1-N_2), in

ambient condition (1-O_2) and under iodine atmosphere (1-I_2),(1-N_2/I_2) unlike in γ-rays. Due to the presence of organic radicals, 1-O_2, 1-I_2, 1-N_2/I_2 showed highest reported conductivity for 2D MHPs (Figure 7c).

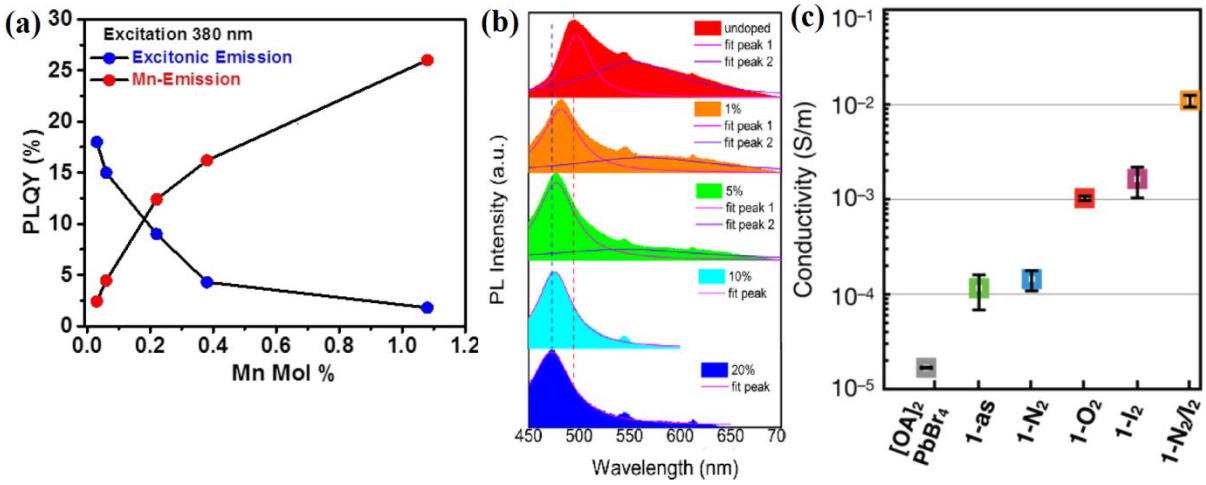

Figure 7: (a) Photoluminescence quantum yield (PLQY) of excitonic and Mn emission in powdered BA_2PbBr_4 with increasing Mn concentrations Reprinted with permission from ref no [92], Copyright 2019 American Chemical Society (b) Room temperature PL spectra of Bi-doped PEA_2SnBr_4 with different Bi concentrations ranging from 0% to 20% in the feed solution Reprinted with permission from ref no [94], Copyright 2019 Elsevier Publishing group (c) Averaged values and standard uncertainties for in-plane conductivity of $[OA]_2PbBr_4$, 1-as, 1-N_2, 1-O_2, 1–I_2 and 1–N_2/I_2 at 423 K Reprinted with permission from ref no [97], Copyright 2018, Wiley-VCH

5. Physical Properties

In this section, some of the fundamental optical and electronic properties of the 2D MHPs are discussed. It is a general observation that because of absence of grain boundaries and lesser defects as compared to polycrystalline film, SCs possess superior properties such as longer diffusion length, longer carrier lifetime, better stability and so forth.

5.1. Optical absorption and Photoluminescence properties

In case of 2D MHP SCs, as the layer thickness *n* increases, band gap decreases owing to the decreased quantum confinement effect and the exciton binding energy reduces because of the dielectric confinement by organic cations. Moreover, in case of very thick crystals PL peak

gets blue shifted as compared to the absorption peak (Figure 8a).[98] By comparing the absorption spectra of polycrystalline films and SCs, the spectra of SCs are smooth and complete with sharp edges, whereas, films show a typical stepwise spectra corresponding to the allowed transitions between quantized electron and hole states (Figure 8b and c).[62] Furthermore, on changing the halide anion from Br to I in $(PEA)_2PbBr_4$, the absorption onset red shifts from 428 nm to 550 nm, which suggests that $(PEA)_2PbI_4$ has wider range of visible light absorption.[55] An interesting observation is presented by Sheikh et. al.[99] The authors reported that $(BA)_2PbI_4$ possess dual optical bandgap, which means that bulk of the SC has lower bandgap with excitonic PL at 2.20eV while the surface and sub-surface layers have higher bandgap with excitonic PL at 2.38eV (Figure 8d).

The photoluminescence quantum yield (PLQY) is defined as the number of photons emitted as a fraction of the number of photons absorbed. The 2D SCs are shown to possess higher PLQY. For instance, $(PEA)_2PbBr_4$ showed PLQY of 22%,[55] which is significantly higher than the polycrystalline film (10%).[100]

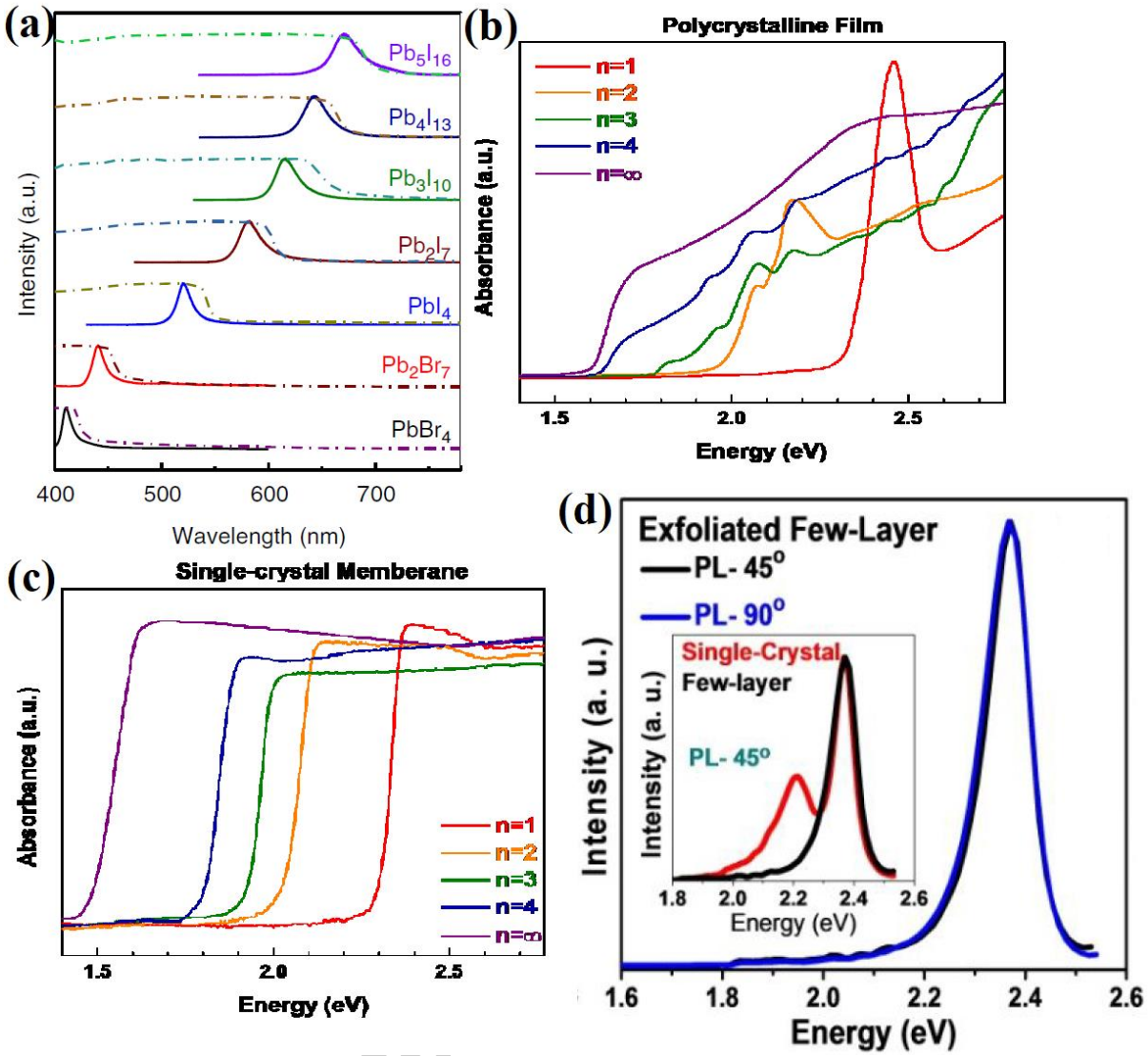

Figure 8: (a) Absorption and photoluminescence spectra of $(BA)_2(MA)_{n-1}Pb_nBr_{3n+1}$ (denoted as Pb_nBr_{3n+1}) and $(BA)_2(MA)_{n-1}Pb_nI_{3n+1}$ (denoted as Pb_nI_{3n+1}) Reprinted with permission from ref no [98], Copyright 2019 Nature Publishing group Comparison of absorption spectra of (b) polycrystalline film and (c) single crystals of quasi 2D $(BA)_2(MA)_{n-1}Pb_nI_{3n+1}$ Reprinted with permission from ref no [62], Copyright 2018 American Chemical Society (d) PL spectra of exfoliated few layer $(BA)_2PbI_4$ with two different excitation angles. The inset compares PL from both single crystal and exfoliated few-layer at 45^o excitation angle Reprinted with permission from ref no [99], Copyright 2018 American Chemical Society

In case of all-inorganic 2D SCs, $Cs_2PbI_2Cl_2$ showed weaker exciton peak unlike in the case of 2D MHPs. It showed a sharp absorption edge at 3.04 eV. However, a small kink was observed in the spectra which can be ascribed to an excitonic absorption. It showed a PL peak at 3.01 eV, which is consistent with the absorption edge. In the temperature dependent PL

spectra as the temperature decreased, a broad peak was observed near the low energy tail, which can be due to self-trapped excitons.[36] McCall et. al., presented a detailed investigation of the optical properties of Bridgman grown SCs of $A_3M_2I_9$ (A = Cs, Rb; M = Bi, Sb), wherein the samples of $Cs_3Sb_2I_9$, $Rb_3Bi_2I_9$, $Rb_3Sb_2I_9$, and $Cs_3Bi_2I_9$ exhibited the band gaps at room temperature of 1.89, 1.93, 2.03 and 2.06 eV, respectively. The colour of the crystals were consistent with the difference in bandgap, for instance, the darkest red crystal of $Cs_3Sb_2I_9$ and lightest red crystal of $Cs_3Bi_2I_9$ exhibited lowest and highest band gaps, respectively. The single crystals of $Cs_3Bi_2I_9$, $Cs_3Sb_2I_9$, and $Rb_3Sb_2I_9$ displayed weak PL emission in the range of 1.58-2.2 eV with line width of 315-403 meV, whereas no emission was evidenced for $Rb_3Bi_2I_9$ at room temperature and even at 15 K. The low temperature PL study revealed several overlapping peaks in the specified range for $Cs_3Bi_2I_9$ at 13K. Conversely, the PL study of $Cs_3Sb_2I_9$ and $Rb_3Sb_2I_9$ revealed a broad near band-edge emission at 1.92 eV and a broad skewed peak at 1.96 eV, respectively at 13 K. The phonon-assisted recombination of the self-trapped excitons (STEs) was responsible for the broad emission in these materials.[71][101]

The SCs of $CsPb_2Br_5$ showed only one absorption edge at 370 nm with bandgap of 3.35 eV. Furthermore, the projected densities of states (PDOS) show that there is no direct contribution of Cs^+ cation to the electronic states. The valance bands near the Fermi level are provided by Br-4p and conduction bands by Pb-6p.[76]

5.2. Carrier lifetime and Carrier mobility

Zhang et. al., provided insights into the properties especially the carrier mobility and anisotropy of 2D SCs utilizing three different spacer cations namely, butylammonium (BA), allylammonium (ALA) and phenethylammonium (PEA).[102] The TRPL measurements revealed that the carrier lifetime τ_2 of $PEA_2MA_2Pb_3I_{10}$ was 19.80 ns, which can be correlated to the decreased exciton binding energy because of the π electrons which can pin the excitonic states to the band edges (Figure 9a).[32] Furthermore, the in-plane mobility (μ_i) of $PEA_2MA_2Pb_3I_{10}$ was found to be 4.4×10^{-2} $cm^2V^{-1}S^{-1}$, which is the largest among the three crystals and the out-of-plane mobility (μ_o) was the smallest with value 1.2×10^{-5} $cm^2V^{-1}S^{-1}$. At the same time, there was not much difference between the μ_o and μ_i for the other two samples, which suggests that π electrons of ALA did not affect the properties of quasi-2D perovskites. The calculated trap density for all the three crystals were 1.1×10^8 cm^{-2}, 1.0×10^8 cm^{-2} and

7.0×10^{7} cm^{-2} for $BA_2MA_2Pb_3I_{10}$, $ALA_2MA_2Pb_3I_{10}$ and $PEA_2MA_2Pb_3I_{10}$, respectively. This indeed suggests that carrier mobility cannot be governed only by the trap density but the organic cation has also influence on it. Xiao et. al., reported that V_I and V_{MA} (vacancy defects) are difficult to form and therefore ion migration along the electric channel is suppressed in quasi 2D perovskites (Figure 9b and c).[65] Li et. al., reported the effect of fluorine substitution in PEA.[103] The results demonstrated that the F atoms act as supramolecular anchor for the neighbouring benzene rings. This effect prevents ion migration and stabilizes crystal. Moreover, the value of free charge carriers decreases because the Fermi level is pushed to the middle of the band gap.

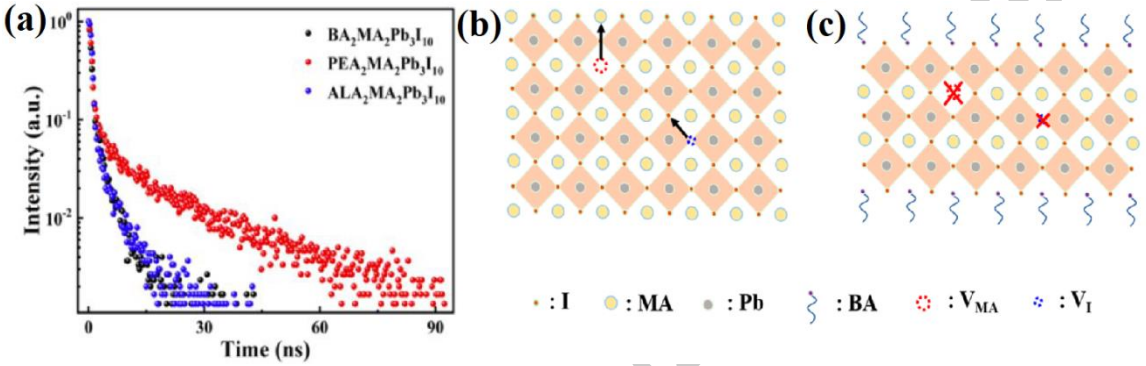

Figure 9: (a) Time-resolved photoluminescence spectra of quasi-2D perovskite single crystals with different spacers Reprinted with permission from ref no [32], Copyright 2020 Wiley-VCH Schemes of the vacancy path for ion migration in (b) 3D and (c) quasi-2D perovskites Reprinted with permission from ref no [65], Copyright 2018 American Chemical Society

6. Conclusions and future outlook

2D SCs are emerging and gaining considerable interest owing to their noteworthy properties that they offer. Up to date, researchers are thoroughly investigating the properties of the 2D polycrystalline films since the first report of 2D perovskite solar cell (PSC) with power conversion efficiency (PCE) ~4%. Currently, the PCE of 2D PSC has reached to ~18%. These materials have been effectively used in various applications such as solar cells, photodetectors, memory devices, LEDs etc.

However, the single crystals of 2D MHPs are still emerging and are in their initial state of development. The crystallization of 2D MHPs is complex and tricky as compared to the 3D MHPs. The reason can be assigned to the unique layered structure induced by bulky organic spacer cation. In this review we have discussed all the methods to synthesize both the hybrid

as well as all inorganic 2DMHPs and their various physical properties. Owing to the amazing optical properties such as fluorescence and exciton effects these SCs are widely utilized in fabricating photodetectors with low dark current and high responsivity. The layered structure gives rise to carrier transport anisotropy which can be beneficial for field effect transistors (FETs). The carrier mobility is higher within inorganic octahedrons compared to the perpendicular plane with organic spacer. Therefore, FETs with surface channel as transport path cam be created. The enhanced stability of these SCs make them suitable for solar cell application however at the same time their wide band gap affects the PCE of the device. Apart from this doping in these SCs provide an additional handle to modulate the PLQY which can be beneficial for LED application. But the following challenges need to be overcome for the future development of 2D SCs and their versatile applications.

1. Most of the existing methods discussed above require careful control of temperature (gradual heating or cooling) and as a result, the time required to synthesize single crystals is too long. There is a need to develop a method which is less time consuming at the same time yields high quality crystals.

2. The choice of solvent also become extremely important as the solubility difference in precursors is large (For ex. PEAI and PbI_2). Therefore, not many options are available to choose from for 2D MHPs.

3. Furthermore, the crystallization methods need to be optimized in a way that large scale production of the 2D MHPs can be made possible. The novel method can also pave a way for the in depth understanding of the properties of 2D SCs and can facilitate their use in various device applications.

4. In case of single crystalline perovskite solar cell, the 3D MHPs have attained PCE of 21.9%, however, in case of 2D SCs, no suitable method is available to fabricate solar cell by the integration of SC with transport layers. It is also worth to find a method to prepare quasi 2D perovskite to improve PCE.

5. The effect of doping of alkali metal cations and heterovalent cations on 2D SCs is not well explored owing to the difficulty in doping as well as in growing doped crystals.

Acknowledgements

P. Y. acknowledges the ORSP of Pandit Deendayal Petroleum University for financial support and the financial support from DST SERB (CRG/2018/000714) and DST Nano Mission (DST/NM/NT/2018/174). On behalf of the entire author P.Y. stated that there is no conflict of interest.

References:

1. A. Mahapatra, D. Prochowicz, M. M. Tavakoli, S. Trivedi, P. Kumar, and P. Yadav, J. Mater. Chem. A **8**, 27 (2020).

2. Best Research Cell Efficiency https://www.nrel.gov/pv/cell-efficiency.html

3. M. M. Tavakoli, P. Yadav, R. Tavakoli, and J. Kong, Adv. Energy Mater. **8**, 1800794 (2018).

4. M. M. Tavakoli, M. Saliba, P. Yadav, P. Holzhey, A. Hagfeldt, S. M. Zakeeruddin, and M. Grätzel, Adv. Energy Mater. **9**, 1802646 (2019).

5. M. M. Tavakoli, R. Tavakoli, P. Yadav, and J. Kong, J. Mater. Chem. A **7**, 679 (2019).

6. R. D. Chavan, M. M. Tavakoli, D. Prochowicz, P. Yadav, S. S. Lote, S. P. Bhoite, A. Nimbalkar, and C. K. Hong, ACS Appl. Mater. Interfaces **12**, 8098 (2020).

7. S. De Wolf, J. Holovsky, S. J. Moon, P. Löper, B. Niesen, M. Ledinsky, F. J. Haug, J. H. Yum, and C. Ballif, J. Phys. Chem. Lett. **5**, 1035 (2014).

8. W. Shockley and H. J. Queisser, J. Appl. Phys. **32**, 510 (1961).

9. P. Yadav, S. H. Turren-Cruz, D. Prochowicz, M. M. Tavakoli, K. Pandey, S. M. Zakeeruddin, M. Grätzel, A. Hagfeldt, and M. Saliba, J. Phys. Chem. C **122**, 15149 (2018).

10. M. M. Tavakoli, H. T. Dastjerdi, D. Prochowicz, P. Yadav, R. Tavakoli, M. Saliba, and Z. Fan, J. Mater. Chem. A **7**, 14753 (2019).

11. D. Prochowicz, M. M. Tavakoli, M. Wolska-Pietkiewicz, M. Jędrzejewska, S. Trivedi, M. Kumar, S. M. Zakeeruddin, J. Lewiński, M. Graetzel, and P. Yadav, Sol. Energy **197**, 50 (2020).

12. R. D. Chavan, P. Yadav, M. M. Tavakoli, D. Prochowicz, A. Nimbalkar, S. P. Bhoite, P. N. Bhosale, and C. K. Hong, Sustain. Energy Fuels **4**, 843 (2020).

13. J. Ding and Q. Yan, Sci. China Mater. **60**, 1063 (2017).

14. R. Babu, L. Giribabu, and S. P. Singh, Cryst. Growth Des. **18**, 2645 (2018).

15. A. Mahapatra, N. Parikh, H. Kumari, M. K. Pandey, M. Kumar, D. Prochowicz, A. Kalam, M. M. Tavakoli, and P. Yadav, J. Appl. Phys. **127**, 185501 (2020).

16. A. Mahapatra, R. Runjhun, J. Nawrocki, J. Lewiński, A. Kalam, P. Kumar, S. Trivedi, M. M. Tavakoli, D. Prochowicz, and P. Yadav, Phys. Chem. Chem. Phys. **22**, 11467 (2020).

17. Y. Dang, Y. Zhou, X. Liu, D. Ju, S. Xia, H. Xia, and X. Tao, Angew. Chemie - Int. Ed. **55**, 3447 (2016).

18. Y. Liu, Z. Yang, D. Cui, X. Ren, J. Sun, X. Liu, J. Zhang, Q. Wei, H. Fan, F. Yu, X. Zhang, C. Zhao, and S. Liu, Adv. Mater. **27**, 5176 (2015).

19. Q. Dong, Y. Fang, Y. Shao, P. Mulligan, J. Qiu, L. Cao, and J. Huang, Science (80). **347**, 967 (2015).

20. S. D. Stranks, G. E. Eperon, G. Grancini, C. Menelaou, M. J. P. Alcocer, T. Leijtens, L. M. Herz, A. Petrozza, and H. J. Snaith, Science (80-.). **342**, 341 (2013).

21. D. Shi, V. Adinolfi, R. Comin, M. Yuan, E. Alarousu, A. Buin, Y. Chen, S. Hoogland, A. Rothenberger, K. Katsiev, Y. Losovyj, X. Zhang, P. A. Dowben, O. F. Mohammed, E. H. Sargent, and O. M. Bakr, Science (80-.). **347**, 519 (2015).

22. J. S. Manser, M. I. Saidaminov, J. A. Christians, O. M. Bakr, and P. V. Kamat, Acc. Chem. Res. **49**, 330 (2016).

23. J. A. Christians, P. A. Miranda Herrera, and P. V. Kamat, J. Am. Chem. Soc. **137**, 1530 (2015).

24. Y. Y. Zhang, S. Chen, P. Xu, H. Xiang, X. G. Gong, A. Walsh, and S. H. Wei, Chinese Phys. Lett. **35**, 036104 (2018).

25. F. Zhang, H. Lu, J. Tong, J. J. Berry, M. C. Beard, and K. Zhu, Energy Environ. Sci. **13**, 1154 (2020).

26. D. Thrithamarassery Gangadharan and D. Ma, Energy Environ. Sci. **12**, 2860 (2019).

27. K. Hong, Q. Van Le, S. Y. Kim, and H. W. Jang, J. Mater. Chem. C **6**, 2189 (2018).

28. A. R. bin M. Yusoff and M. K. Nazeeruddin, Adv. Energy Mater. **8**, 1702073 (2018).

29. N. Parikh, M. M. Tavakoli, M. K. Pandey, A. Kalam, D. Prochowicz, and P. K. Yadav, Sustain. Energy Fuels (2021).

30. L. Mao, C. C. Stoumpos, and M. G. Kanatzidis, J. Am. Chem. Soc. **141**, 1171 (2019).

31. P. Gao, A. R. Bin Mohd Yusoff, and M. K. Nazeeruddin, Nat. Commun. **9**, 5028 (2018).

32. N. Zhou, B. Huang, M. Sun, Y. Zhang, L. Li, Y. Lun, X. Wang, J. Hong, Q. Chen, and H. Zhou, Adv. Energy Mater. **10**, 1901566 (2020).

33. J. Zhang, L. Zhang, X. Li, X. Zhu, J. Yu, and K. Fan, ACS Sustain. Chem. Eng. **7**, 3487 (2019).

34. Y. Li, H. Cheng, K. Zhao, and Z. S. Wang, ACS Appl. Mater. Interfaces **11**, 37804 (2019).

35. I. C. Smith, E. T. Hoke, D. Solis-Ibarra, M. D. McGehee, and H. I. Karunadasa, Angew. Chemie - Int. Ed. **53**, 11232 (2014).

36. J. Li, Q. Yu, Y. He, C. C. Stoumpos, G. Niu, G. G. Trimarchi, H. Guo, G. Dong, D. Wang, L. Wang, and M. G. Kanatzidis, J. Am. Chem. Soc. **140**, 11085 (2018).

37. J. Di, J. Chang, and S. (Frank) Liu, EcoMat **2**, 1 (2020).

38. D. B. Mitzi, J. Chem. Soc. Dalt. Trans. **0**, 1 (2001).

39. B. Saparov and D. B. Mitzi, Chem. Rev. **116**, 4558 (2016).

40. X. D. Liu, Q. Wang, Z. Q. Cheng, Y. H. Qiu, L. Zhou, and Q. Q. Wang, Mater. Lett. **206**, 75 (2017).

41. X. Sheng, G. Chen, C. Wang, W. Wang, J. Hui, Q. Zhang, K. Yu, W. Wei, M. Yi, M. Zhang, Y. Deng, P. Wang, X. Xu, Z. Dai, J. Bao, and X. Wang, Adv. Funct. Mater. **28**, 1800283 (2018).

42. S. T. Ha, X. Liu, Q. Zhang, D. Giovanni, T. C. Sum, and Q. Xiong, Adv. Opt. Mater. **2**,

838 (2014).

43. N. Zhou, Y. Shen, L. Li, S. Tan, N. Liu, G. Zheng, Q. Chen, and H. Zhou, J. Am. Chem. Soc. **140**, 459 (2018).

44. M. Yuan, L. N. Quan, R. Comin, G. Walters, R. Sabatini, O. Voznyy, S. Hoogland, Y. Zhao, E. M. Beauregard, P. Kanjanaboos, Z. Lu, D. H. Kim, and E. H. Sargent, Nat. Nanotechnol. **11**, 872 (2016).

45. B. Vargas, R. Torres-Cadena, J. Rodríguez-Hernández, M. Gembicky, H. Xie, J. Jiménez-Mier, Y. S. Liu, E. Menéndez-Proupin, K. R. Dunbar, N. Lopez, P. Olalde-Velasco, and D. Solis-Ibarra, Chem. Mater. **30**, 5315 (2018).

46. X. Zhang, X. Ren, B. Liu, R. Munir, X. Zhu, D. Yang, J. Li, Y. Liu, D. M. Smilgies, R. Li, Z. Yang, T. Niu, X. Wang, A. Amassian, K. Zhao, and S. Liu, Energy Environ. Sci. **10**, 2095 (2017).

47. L. Mao, W. Ke, L. Pedesseau, Y. Wu, C. Katan, J. Even, M. R. Wasielewski, C. C. Stoumpos, and M. G. Kanatzidis, J. Am. Chem. Soc. **140**, 3775 (2018).

48. C. Ortiz-Cervantes, P. Carmona-Monroy, and D. Solis-Ibarra, ChemSusChem **12**, 1560 (2019).

49. A. Poglitsch and D. Weber, J. Chem. Phys. **87**, 6373 (1987).

50. Y. Dang, Y. Liu, Y. Sun, D. Yuan, X. Liu, W. Lu, G. Liu, H. Xia, and X. Tao, CrystEngComm **17**, 665 (2015).

51. C. C. Stoumpos, D. H. Cao, D. J. Clark, J. Young, J. M. Rondinelli, J. I. Jang, J. T. Hupp, and M. G. Kanatzidis, Chem. Mater. **28**, 2852 (2016).

52. W. Peng, J. Yin, K. T. Ho, O. Ouellette, M. De Bastiani, B. Murali, O. El Tall, C. Shen, X. Miao, J. Pan, E. Alarousu, J. H. He, B. S. Ooi, O. F. Mohammed, E. Sargent, and O. M. Bakr, Nano Lett. **17**, 4759 (2017).

53. L. Mao, W. Ke, L. Pedesseau, Y. Wu, C. Katan, J. Even, M. R. Wasielewski, C. C. Stoumpos, and M. G. Kanatzidis, J. Am. Chem. Soc. **140**, 3775 (2018).

54. C. M. Raghavan, T. P. Chen, S. S. Li, W. L. Chen, C. Y. Lo, Y. M. Liao, G. Haider, C. C. Lin, C. C. Chen, R. Sankar, Y. M. Chang, F. C. Chou, and C. W. Chen, Nano Lett. **18**, 3221

(2018).

55. Y. Zhang, Y. Liu, Z. Xu, H. Ye, Q. Li, M. Hu, Z. Yang, and S. Liu, J. Mater. Chem. C **7**, 1584 (2019).

56. M. Xiao, F. Huang, W. Huang, Y. Dkhissi, Y. Zhu, J. Etheridge, A. Gray-Weale, U. Bach, Y. B. Cheng, and L. Spiccia, Angew. Chemie - Int. Ed. **53**, 9898 (2014).

57. N. J. Jeon, J. H. Noh, Y. C. Kim, W. S. Yang, S. Ryu, and S. Il Seok, Nat. Mater. **13**, 897 (2014).

58. H. Tian, L. Zhao, X. Wang, Y. W. Yeh, N. Yao, B. P. Rand, and T. L. Ren, ACS Nano **11**, 12247 (2017).

59. F. Lédée, G. Trippé-Allard, H. Diab, P. Audebert, D. Garrot, J. S. Lauret, and E. Deleporte, CrystEngComm **19**, 2598 (2017).

60. A. A. Zhumekenov, V. M. Burlakov, M. I. Saidaminov, A. Alofi, M. A. Haque, B. Turedi, B. Davaasuren, I. Dursun, N. Cho, A. M. El-Zohry, M. De Bastiani, A. Giugni, B. Torre, E. Di Fabrizio, O. F. Mohammed, A. Rothenberger, T. Wu, A. Goriely, and O. M. Bakr, ACS Energy Lett. **2**, 1782 (2017).

61. Y. Liu, H. Ye, Y. Zhang, K. Zhao, Z. Yang, Y. Yuan, H. Wu, G. Zhao, Z. Yang, J. Tang, Z. Xu, and S. (Frank) Liu, Matter **1**, 465 (2019).

62. K. Wang, C. Wu, D. Yang, Y. Jiang, and S. Priya, ACS Nano **12**, 4919 (2018).

63. Z. Chen, B. Turedi, A. Y. Alsalloum, C. Yang, X. Zheng, I. Gereige, A. Alsaggaf, O. F. Mohammed, and O. M. Bakr, ACS Energy Lett. **4**, 1258 (2019).

64. A. Y. Alsalloum, B. Turedi, X. Zheng, S. Mitra, A. A. Zhumekenov, K. J. Lee, P. Maity, I. Gereige, A. AlSaggaf, I. S. Roqan, O. F. Mohammed, and O. M. Bakr, ACS Energy Lett. **5**, 657 (2020).

65. X. Xiao, J. Dai, Y. Fang, J. Zhao, X. Zheng, S. Tang, P. N. Rudd, X. C. Zeng, and J. Huang, ACS Energy Lett. **3**, 684 (2018).

66. Y. Liu, Y. Zhang, Z. Yang, H. Ye, J. Feng, Z. Xu, X. Zhang, R. Munir, J. Liu, P. Zuo, Q. Li, M. Hu, L. Meng, K. Wang, D.-M. Smilgies, G. Zhao, H. Xu, Z. Yang, A. Amassian, J. Li, K. Zhao, and S. Liu, Nat. Commun. **9**, 5302 (2018).

67. X. He, Y. Wang, K. Li, X. Wang, P. Liu, Y. Yang, Q. Liao, T. Zhai, J. Yao, and H. Fu, ACS Appl. Mater. Interfaces **11**, 15905 (2019).

68. Z. Gu, Z. Huang, C. Li, M. Li, and Y. Song, Sci. Adv. **4**, eaat2390 (2018).

69. J. Wang, C. Fang, J. Ma, S. Wang, L. Jin, W. Li, and D. Li, ACS Nano **13**, 9473 (2019).

70. S. A. Fateev, A. A. Petrov, A. A. Ordinartsev, A. Y. Grishko, E. A. Goodilin, and A. B. Tarasov, Chem. Mater. **32**, 9805 (2020).

71. K. M. McCall, C. C. Stoumpos, S. S. Kostina, M. G. Kanatzidis, and B. W. Wessels, Chem. Mater. **29**, 4129 (2017).

72. K. M. McCall, C. C. Stoumpos, O. Y. Kontsevoi, G. C. B. Alexander, B. W. Wessels, and M. G. Kanatzidis, Chem. Mater. **31**, 2644 (2019).

73. A. Y. Tarasova, L. I. Isaenko, V. G. Kesler, V. M. Pashkov, A. P. Yelisseyev, N. M. Denysyuk, and O. Y. Khyzhun, J. Phys. Chem. Solids **73**, 674 (2012).

74. P. Acharyya, T. Ghosh, K. Pal, K. Kundu, K. Singh Rana, J. Pandey, A. Soni, U. V. Waghmare, and K. Biswas, J. Am. Chem. Soc. **142**, 15595 (2020).

75. X. Li, S. Wang, S. Zhao, L. Li, Y. Li, B. Zhao, Y. Shen, Z. Wu, P. Shan, and J. Luo, Chem. - A Eur. J. **24**, 9243 (2018).

76. I. Dursun, M. De Bastiani, B. Turedi, B. Alamer, A. Shkurenko, J. Yin, A. M. El-Zohry, I. Gereige, A. AlSaggaf, O. F. Mohammed, M. Eddaoudi, and O. M. Bakr, ChemSusChem **10**, 3746 (2017).

77. M. Usman and Q. Yan, Cryst. Growth Des. **21**, 579 (2020).

78. X. Zhang, L. Li, Z. Sun, and J. Luo, Chem. Soc. Rev. **48**, 517 (2019).

79. Y. Zhou, J. Chen, O. M. Bakr, and H. T. Sun, Chem. Mater. **30**, 6589 (2018).

80. M. V. Kovalenko, L. Protesescu, and M. I. Bodnarchuk, Science (80-.). **358**, 745 (2017).

81. N. Pradhan, S. Das Adhikari, A. Nag, and D. D. Sarma, Angew. Chemie - Int. Ed. **56**, 7038 (2017).

82. A. J. Houtepen, Z. Hens, J. S. Owen, and I. Infante, Chem. Mater. **29**, 752 (2017).

83. P. Yadav, M. I. Dar, N. Arora, E. A. Alharbi, F. Giordano, S. M. Zakeeruddin, and M. Grätzel, Adv. Mater. **29**, 1701077 (2017).

84. Y. Zhou, Z. J. Yong, W. Zhang, J. P. Ma, A. Sadhanala, Y. M. Chen, B. M. Liu, Y. Zhou, B. Song, and H. T. Sun, J. Mater. Chem. C **5**, 2591 (2017).

85. Z. Tang, T. Bessho, F. Awai, T. Kinoshita, M. M. Maitani, R. Jono, T. N. Murakami, H. Wang, T. Kubo, S. Uchida, and H. Segawa, Sci. Rep. **7**, 12183 (2017).

86. D. Parobek, B. J. Roman, Y. Dong, H. Jin, E. Lee, M. Sheldon, and D. H. Son, Nano Lett. **16**, 7376 (2016).

87. Q. Hu, Z. Li, Z. Tan, H. Song, C. Ge, G. Niu, J. Han, and J. Tang, Adv. Opt. Mater. **6**, 1700864 (2018).

88. J. S. Yao, J. Ge, B. N. Han, K. H. Wang, H. Bin Yao, H. L. Yu, J. H. Li, B. S. Zhu, J. Z. Song, C. Chen, Q. Zhang, H. B. Zeng, Y. Luo, and S. H. Yu, J. Am. Chem. Soc. **140**, 3626 (2018).

89. B. Ghosh and R. K. Mukherjee, Phys. Status Solidi **102**, 189 (1980).

90. A. Biswas, R. Bakthavatsalam, and J. Kundu, Chem. Mater. **29**, 7816 (2017).

91. R. Bakthavatsalam, A. Biswas, M. Chakali, P. R. Bangal, B. P. Kore, and J. Kundu, J. Phys. Chem. C **123**, 4739 (2019).

92. T. Sheikh and A. Nag, J. Phys. Chem. C **123**, 9420 (2019).

93. S. K. Dutta, A. Dutta, S. Das Adhikari, and N. Pradhan, ACS Energy Lett. **4**, 343 (2019).

94. R. Zhang, X. Mao, P. Cheng, Y. Yang, S. Yang, T. Wumaier, W. Deng, and K. Han, J. Energy Chem. **36**, 1 (2019).

95. J. M. Richter, M. Abdi-Jalebi, A. Sadhanala, M. Tabachnyk, J. P. H. Rivett, L. M. Pazos-Outón, K. C. Gödel, M. Price, F. Deschler, and R. H. Friend, Nat. Commun. **7**, 13941 (2016).

96. L. M. Pazos-Outón, M. Szumilo, R. Lamboll, J. M. Richter, M. Crespo-Quesada, M. Abdi-Jalebi, H. J. Beeson, M. Vrućinić, M. Alsari, H. J. Snaith, B. Ehrler, R. H. Friend, and F. Deschler, Science (80). **351**, 1430 (2016).

97. C. Ortiz-Cervantes, P. I. Román-Román, J. Vazquez-Chavez, M. Hernández-Rodríguez,

and D. Solis-Ibarra, Angew. Chemie - Int. Ed. **57**, 13882 (2018).

98. J. Li, J. Wang, J. Ma, H. Shen, L. Li, X. Duan, and D. Li, Nat. Commun. **10**, 806 (2019).

99. T. Sheikh, A. Shinde, S. Mahamuni, and A. Nag, ACS Energy Lett. **3**, 2940 (2018).

100. D. Liang, Y. Peng, Y. Fu, M. J. Shearer, J. Zhang, J. Zhai, Y. Zhang, R. J. Hamers, T. L. Andrew, and S. Jin, ACS Nano **10**, 6897 (2016).

101. P. Acharyya, K. Kundu, and K. Biswas, Nanoscale **12**, 21094 (2020).

102. Y. Zhang, M. Sun, N. Zhou, B. Huang, and H. Zhou, J. Phys. Chem. Lett. **11**, 7610 (2020).

103. H. Li, J. Song, W. Pan, D. Xu, W. Zhu, H. Wei, and B. Yang, Adv. Mater. **32**, 2003790 (2020).